J Comput Neurosci (2008) 24:37–55
DOI 10.1007/s10827-007-0040-z

Using phase resetting to predict 1:1 and 2:2 locking in two neuron networks in which firing order is not always preserved

Selva K. Maran · Carmen C. Canavier

Received: 28 August 2006 / Revised: 12 April 2007 / Accepted: 16 April 2007 / Published online: 19 June 2007

Abstract Our goal is to understand how nearly synchronous modes arise in heterogenous networks of neurons. In heterogenous networks, instead of exact synchrony, nearly synchronous modes arise, which include both 1:1 and 2:2 phase-locked modes. Existence and stability criteria for 2:2 phase-locked modes in reciprocally coupled two neuron circuits were derived based on the open loop phase resetting curve (PRC) without the assumption of weak coupling. The PRC for each component neuron was generated using the change in synaptic conductance produced by a presynaptic action potential as the perturbation. Separate derivations were required for modes in which the firing order is preserved and for those in which it alternates. Networks composed of two model neurons coupled by reciprocal inhibition were examined to test the predictions. The parameter regimes in which both types of nearly synchronous modes are exhibited were accurately predicted both qualitatively and quantitatively provided that the synaptic time constant is short with respect to the period and that the effect of second order resetting is considered. In contrast, PRC methods based on weak coupling could not predict 2:2 modes and did not predict the 1:1 modes with the level of accuracy achieved by the strong coupling methods. The strong coupling prediction methods provide insight into what manipulations promote near-synchrony in a two neuron network and may also have predictive value for larger networks, which can also manifest changes in firing order. We also identify a novel route by which synchrony is lost in mildly heterogenous networks.

Keywords Synchrony · Phase response curve · Network oscillation

Action Editor: David Terman

S. K. Maran · C. C. Canavier
Neuroscience Center for Excellence, LSU Health Sciences Center, New Orleans, LA 70112, USA

C. C. Canavier
Department of Ophthalmology, LSU Health Sciences Center, New Orleans, LA 70112, USA

C. C. Canavier (✉)
LSU Health Sciences Center, 2020 Gravier Street, Suite D, New Orleans, LA 70112, USA
e-mail: ccanav@lsuhsc.edu

1 Introduction

The application of phase resetting theory to the prediction of network activity is an example of where theory meets experiment, because the phase resetting curve can easily be obtained experimentally in order to characterize physiological neurons. Phase resetting methods are applied directly to the experimental data thus they are model-independent and widely applicable. However, they are limited to situations in which their underlying assumptions are not violated. In this study, these limits are more clearly established, in part to pave the way for improvements in the theory. A complete understanding of how the phase resetting curves influence synchronization and phase-locking, coupled with an understanding of how the intrinsic and synaptic currents determine the phase resetting curve, would allow control of synchronization properties by targeting specific conductances.

Although the PRC methods are general, in this study a simple network of inhibitory neurons is used as an example in order to illustrate the methods. Inhibitory interneurons play an essential role in the generation and control of synchronous oscillations in the brain (Whittington et al. 1995). In heterogenous networks, instead of exact synchrony,

nearly synchronous modes arise [Fig. 1(a)] (Skinner et al. 2005b). In the simplest inhibitory network consisting of two reciprocally coupled neurons, these nearly synchronous modes include 1:1 phase-locking at small phases and also *n*:*n* phase-locking, in which the interval between the firing of the two neurons is not the same every cycle, but repeats every n cycles. In this study we observe both 1:1 and 2:2 lockings. Within these 2:2 lockings, firing order can be preserved [Fig. 1(c)] or not [Fig. 1(d)]. Previous criteria for the stability of phase-locking based on the open loop phase response curves (PRC) of the individual neurons have been developed for 1:1 phase-locking such as near synchronous or near antiphase [Fig. 1(b)] as (Dror et al. 1999; Oprisan and Canavier 2001; Oprisan et al. 2004) in networks of two neurons. These methods have been tested on both model neurons (Canavier et al. 1997, 1999; Luo et al. 2004) and hybrid networks (Netoff et al. 2005b; Oprisan et al. 2004). Our aim here is to develop and test criteria for the existence and stability of 2:2 steady phase-locked modes in reciprocally coupled two neuron circuits based on the open loop phase response curve (PRC) of the component neurons to the synaptic input. The prediction of 2:2 modes is a rigorous quantitative test of the PRC methods that do not assume weak coupling.

The main assumption is that each neuron returns close to its unperturbed cycle and that the phase resetting due to the previous input is complete before its next input is received, thus allowing the application of PRC curves generated in the open loop configuration to the prediction of closed loop network activity. The second assumption is that the input received in the circuit is similar to the input used to generate the open loop PRC, here assumed to be an action potential in the presynaptic neuron. The synaptic coupling in inhibitory networks has a time constant on the order of a few ms, hence a synaptic input delivered shortly before an action potential is fired can still be active after the action potential and therefore its influence can span two cycles [see Fig. 2(b)]. Consequently, the PRC methods must take into account resetting that occurs in the cycle that contains the perturbation (first order) and the next cycle (second order). According to the main assumption, the second order resetting is assumed to be complete by the time the next input is received. Experimental studies have shown the existence of second order resetting (Reyes and Fetz 1993) in cortical neurons, in stellate cells (Netoff et al. 2005a), in heart cell aggregates (Guevara et al. 1986), and in invertebrate neurons (Preyer and Butera 2005), and recent studies (Netoff et al. 2005b; Oprisan et al. 2004) using hybrid networks of one biological and one model neuron suggest that accounting for second order resetting is necessary. In addition to the PRC methods presented here, PRC methods based on assumptions of weak coupling and mild heterogeneity have been widely applied, so we will compare the results of the two approaches here, with the caveat that the presence of second order resetting implies that the weak coupling method may not apply.

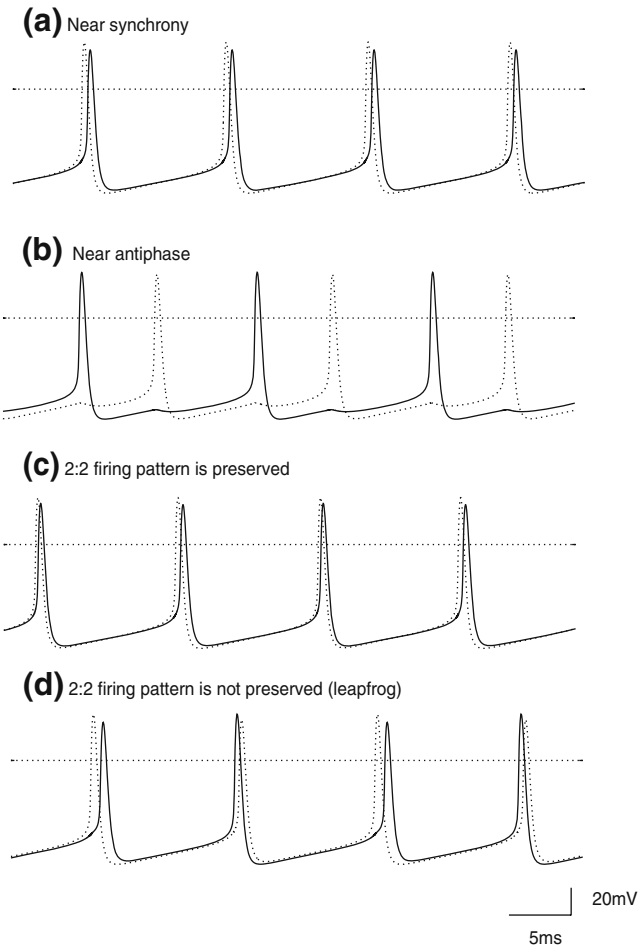

Fig. 1 Typical modes exhibited in a two neuron network. (**a**) 1P near synchronous mode with 1:1 locking and alternating firing. (**b**) Another 1:1 locking with alternating firing near antiphase. (**c**) 2P mode with 2:2 locking and alternating firing in which the order remains constant. (**d**) A type of 2P mode in which the firing order changes each cycle in a "leapfrog" fashion. (**a**, **c** and **d**) are "nearly synchronous" while (**b**) is not. The parameter values were g_{syn}=0.35 mS/cm^2 and τ_{syn}=1 ms, I_{app}=2.0 μA/cm^2 with ε=0.11 μA/cm^2 for panel (**a**), 0.04 μA/cm^2 for panel (**b**), 0.082 μA/cm^2 for panel (**c**), and 0.015 μA/cm^2 for panel (**d**). The *dotted lines* indicate 0 mV

2 Materials and methods

2.1 Wang and Buzsáki model

In order to test the prediction methods described below, a network comprised of two single compartment Wang and Buzsáki (1996) model cortical interneurons was used. More complex and physiologically realistic models are available, but this model was chosen as the platform for testing PRC

methods because of its simplicity. The method presented herein is independent of model details because only the numerically generated PRC is utilized in the predictions. The model neurons were reciprocally coupled by identical inhibitory synapses. The differential equations for each neuron are

$$C\,dV/dt = -I_{Na} - I_K - I_L - I_{syn} + I_{stim}$$
$$dh/dt = \phi\{\alpha_h(V)(1-h) - \beta_h(V)h\}$$
$$dn/dt = \phi\{\alpha_n(V)(1-n) - \beta_n(V)n\}$$

where the capacitance C=1 μF/cm^2, V is the cell membrane voltage in millivolts, t is time in milliseconds and ϕ=5. $I_L=g_L(V-E_L)$ is the leak current. The sodium current is given by $I_{Na}=g_{Na}m_\infty^3 h(V-E_{Na})$. The steady-state activation is $m_\infty=\alpha_m/(\alpha_m+\beta_m)$ where $\alpha_m(V)=-0.1(V+35)/\{\exp[-0.1(V+35)]-1\}$, $\beta_m(V)=4\exp[-(V+60)/18]$. The rate constants for the inactivation variable h are $\alpha_h(V)=0.07\exp[-(V+58)/20]$, $\beta_h(V)=1/\{\exp[-0.1(V+28)]+1\}$. The potassium current is $I_K=g_K\,n^4\,(V-E_K)$, where the rate constants for n are $\alpha_n(V)=-0.01(V+34)/(\exp[-0.1(V+34)]-1\}$, $\beta_n(V)=0.125\exp[-(V+44)/80]$. Maximal sodium ($g_{Na}$), potassium ($g_K$) and leak ($g_L$) conductances were set to 35, 9, and 0.1 mS/cm^2, respectively. The reversal potentials E_{Na}, E_K, and E_L were set to 55, −90, and −65 mV, respectively.

The synaptic current is given by $I_{syn}=g_{syn}s(V-E_{syn})$, where g_{syn} is the maximum synaptic conductance and E_{syn}=−75 mV is the reversal potential. The rate of change of the gating variable s is $ds/dt=\alpha T(V_{pre})(1-s)-s/\tau_{syn}$, and $T(V_{pre})=1/[1+\exp(-V_{pre}/2)]$, where V_{pre} is the voltage of the presynaptic cell, α=6.25 ms^{-1} is the rate constant of the synaptic activation (Bartos et al. 2001), and τ_{syn} is the synaptic decay time constant.

Heterogeneity was introduced by varying the applied current I_{stim} (in μA/cm^2) such that $I_{stim,1}=I_{app}+\varepsilon$ and $I_{stim,2}=I_{app}-\varepsilon$, giving neuron 1 a faster frequency than neuron 2. In the 10 neuron network simulations $I_{stim,n}=I_{app}-\varepsilon+(2n\varepsilon)/9$, where n ranges from 0 to 9. The values of τ_{syn}, I_{app}, ε, g_{syn} were varied in order to explore the parameter space. The set of initial conditions with $h_1=h_2$=0.9379, $n_1=n_2$=0.1224, $s_1=s_2$=0.1386, and $V_1=V_2$=−59.5567 often produced near synchronous modes in two neuron and 10 neuron networks, whereas V_1=−58.7249, V_2=−55.0456 often produced near antiphase modes in two neuron network. For 10 neuron network the V_1=−59.5567 for neurons with odd number and V_2=−51.5567 for neurons with even number produced near antiphase modes. The differential equations were solved using a variable step size, fifth order implicit Runge Kutta method using a packaged Fortran subroutine (Hairer and Wanner 1991) and drivers that we wrote in C.

2.2 Computation of the phase resetting curve

Figure 2(a) illustrates how the PRC is computed. The presynaptic cell is initialized at its threshold at different points

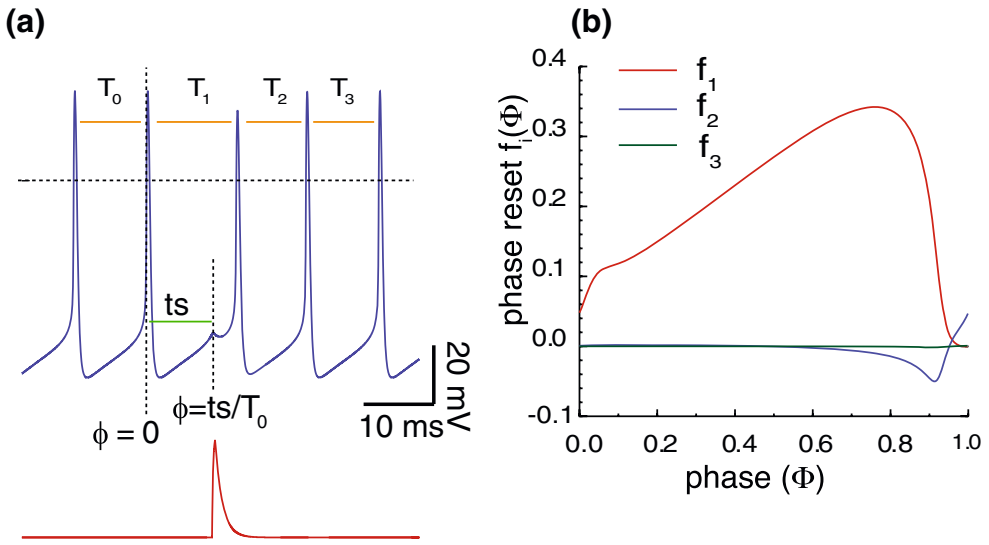

Fig. 2 Phase resetting curve. (**a**) The phase resetting curve is generated using an action potential from the presynaptic neuron as the perturbation. The unperturbed cycle period is T_0. The duration of the cycle that contains the perturbation is T_1, the subsequent one is T_2, and the one after that is T_3. The phase at which a stimulus is received is φ=ts/P_i, where P_i is the intrinsic period of the postsynaptic neuron and ts is the time interval between the last action potential and the synaptic input perturbation. The phase resetting curve (PRC) is given by $f_i(\varphi)=(T_i-T)/T$. The *dotted line* indicates 0 mV. The *red trace* shows the timing of the perturbation in synaptic conductance produced by a presynaptic action potential. (**b**) Characteristic shapes of the $f_1(\varphi)$, $f_2(\varphi)$, and $f_3(\varphi)$ phase resetting curves. Note that $f_3(\varphi)$ is nearly zero, and that the sum of $f_1(\varphi)$ and $f_2(\varphi)$ is continuous at 0 and 1. The parameter values were g_{syn}=0.35 mS/cm^2 and τ_{syn}=1 ms, I_{app}=2.0 μA/cm^2 and ε=0.07 μA/cm^2. The PRC is given for the faster neuron

in the cycle of the post-synaptic cell. The action potential threshold was set to −14 mV in this study, such that a phase of zero was associated with the membrane potential crossing −14 mV as it is increasing. The single action potential in the pre-synaptic cell triggers a change in synaptic conductance [bottom trace, Fig. 2(a)] that serves as the perturbation utilized to generate the PRC. In the open loop condition the phase at which a stimulus is received is φ=ts/P_i, where P_i is the intrinsic period and ts is the time between the last action potential in the neuron for which the PRC is being generated and the action potential initiation in the presynaptic neuron. The normalized change in the length of the cycle containing the perturbation was called first order resetting [$f_1(\phi)$], that in the next cycle second order resetting, and that in the following cycle third order. This can be summarized as $f_i(\phi)=(T_i-T_0)/T_0$, where T_0 for the unperturbed cycle is equal to the intrinsic free running period P_i. In order for the assumption of a quick return to the limit cycle to be satisfied, $f_3(\phi)$ should be near zero, as it is in Fig. 2(b), and the sum of $f_1(\phi)$ and $f_2(\phi)$ should be continuous at 0 and 1 [as it is in Fig. 2(b)]. The shape of $f_1(\phi)$ is largely invariant to changes in frequency. This is because the Wang and Buzsáki model is an integrator in a Class I excitability regime (Ermentrout 1996), and the phase resetting caused by a perturbation in current is determined by the shape of the limit cycle, which is invariant to changes in frequency for Type I oscillators (Oprisan and Canavier 2002).

2.3 Emulator

In order to determine if the PRCs generated above contained all the information necessary to predict the patterns generated by networks comprised of the neurons in the reciprocally coupled conditions, an emulator algorithm (Canavier et al. 1999) was employed. The inputs to the emulator are the phase resetting curve for each presynaptic–postsynaptic pair, the intrinsic period of each oscillator, and the initial phase of each oscillator. The emulator determines which neuron(s) will fire next by determining which neuron(s) has the shortest time remaining until it reaches a phase of one. Each neuron j that does not fire at this time has its phase incremented by the normalized time to the next spike, then the first order resetting due to the current spike(s) in its presynaptic neuron(s) k that do fire at this time is subtracted from its phase. The second order resetting due to the current spike(s) is added to any second order resetting that has occurred since neuron j last fired. Then the neuron(s) k that fire have their phase reset to zero and any accumulated second order resetting is subtracted from the phase. The emulator effectively reduces the neural circuit to a set of coupled nonlinear maps.

2.4 Periodicity and stability criteria

The emulator is difficult to formulate analytically. In order make a priori predictions from the PRCS about whether a particular pattern is a stable solution of the discrete system described by the emulator, and by analogy of the differential equations that describe the couple circuit, a firing pattern must be assumed. In this section we assume firing patterns for two types of 2:2 modes and derive existence and stability criteria. The idea is simply to use phase resetting theory to formulate algebraic expressions for the intervals between successive neural firings in terms of the previous intervals, then to linearize about a presumed fixed point in which the phasic relationships are constant, and to use linear systems theory to determine the stability of the locking. In the linearized system, stability is determined by the slopes of the PRC at the locking points.

The assumed firing pattern for a 2:2 locking in which the firing order is preserved is given in Fig. 3(a). The stimulus intervals (ts_{ij}) represent the time elapsed between the firing of neuron i and the reception of the input j from the other neuron. The recovery intervals (tr_{ij}) represent the time elapsed between the receipt of the input j by neuron i and the next spike fired by neuron i. The assumed firing pattern implies that the following intervals must be equal by definition.

$$ts_{11}[n] = tr_{22}[n];\ ts_{12}[n] = tr_{21}[n];\ ts_{21} = tr_{11};\ ts_{22}[n] = tr_{12}[n]$$

Their steady state counterparts at $n=\infty$ must be equal in order for a locked mode to exist. Note that the designation of one pair of stimulus intervals as $ts_{11}[n]$ and $ts_{22}[n]$ and the other pair as $ts_{12}[n]$ and $ts_{21}[n]$ is arbitrary. Qualitatively, they are identical and these pairs are interchangeable, which produces symmetry in the solution structure. Since the firing order does not change, all 1P solutions in which $ts_{11}[\infty]=ts_{12}[\infty]$ and $ts_{21}[\infty]=ts_{22}[\infty]$ will satisfy this pattern and will be solutions to a mapping based on Fig. 3(a). Furthermore, if a solution is found in which $ts_{11}[\infty]=x_1$, $ts_{12}[\infty]=x_2$, $ts_{21}[\infty]=x_3$, and $ts_{22}[\infty]=x_4$, then $ts_{11}[\infty]=x_2$, $ts_{12}[\infty]=x_1$, $ts_{21}[\infty]=x_4$, and $ts_{22}[\infty]=x_3$ is also a solution due to symmetry.

The stimulus intervals in a steady state phase-locked 2P mode can be computed by multiplying the appropriate intrinsic period P_i by the phase of the neuron when input j is received (ϕ_{ij}) plus the amount of second order resetting $f_{2i}(\phi)$ due to the previous input that occurs after the most recent spike in neuron i. The recovery interval is determined by the amount of time remaining until the next spike if no input were received, which is $P_i\{1-\phi\}$, plus the first order resetting attributable to an input received at that phase $f_{1i}(\phi)$. Combining the expressions for intervals known to

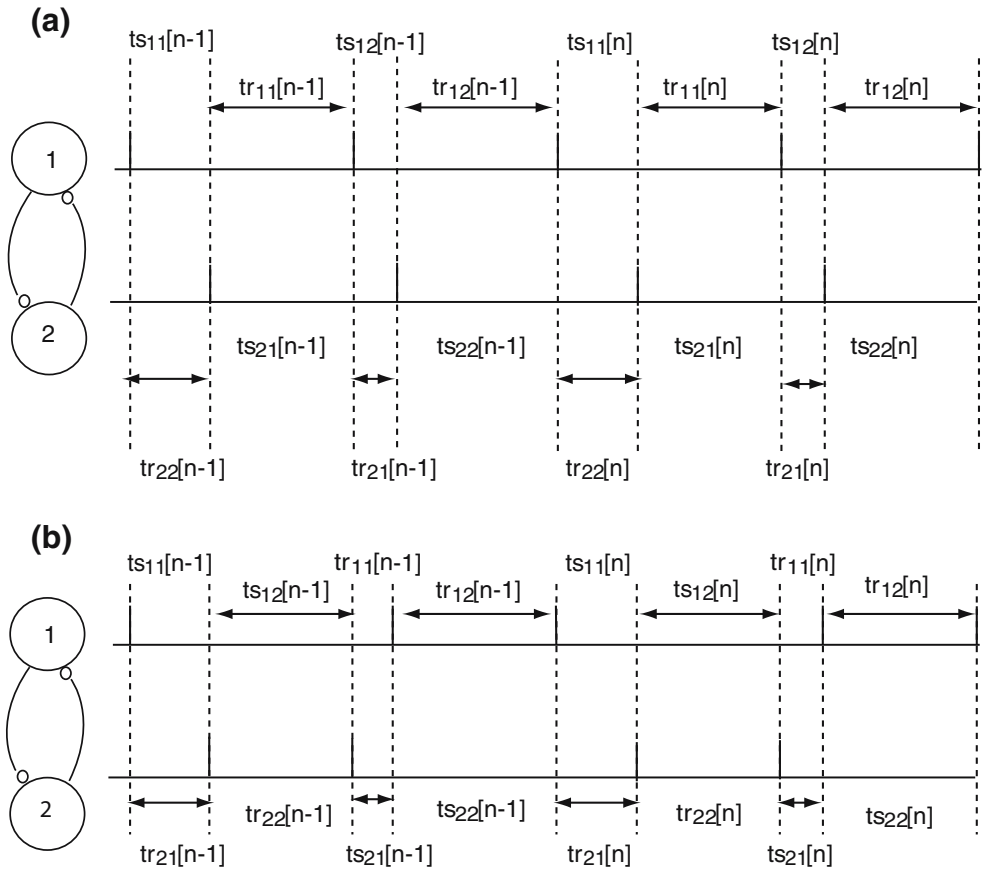

Fig. 3 Firing pattern for 2:2 lockings. (**a**) Firing order is preserved. The ts_{ij} in the *figure above* represent stimulus intervals and the tr_{ij} represent recovery intervals (see text). (**b**) Firing order is not preserved. Note that the firing order changes on every cycle. The definitions for the ts_{ij} and tr_{ij} are different than in (**a**) because the assumed firing pattern is different (see text)

be equal in a steady state mode yields the following mapping

$$\begin{aligned} ts_{11}[n] &= tr_{22}[n];\ P_1\{\phi_{11}[n] + f_{21}(\phi_{12}[n-1])\} \\ &= P_2\{1 - \phi_{22}[n-1] + f_{12}(\phi_{22}[n-1])\} \end{aligned} \quad (1)$$

$$\begin{aligned} ts_{12}[n] &= tr_{21}[n];\ P_1\{\phi_{12}[n] + f_{21}(\phi_{11}[n])]\} \\ &= P_2\{1 - \phi_{21}[n] + f_{12}(\phi_{21}[n])\} \end{aligned} \quad (2)$$

$$\begin{aligned} ts_{21}[n] &= tr_{11}[n];\ P_2\{\phi_{21}[n] + f_{22}(\phi_{22}[n-1])\} \\ &= P_1\{1 - \phi_{11}[n] + f_{11}(\phi_{11}[n])\} \end{aligned} \quad (3)$$

$$\begin{aligned} ts_{22}[n] &= tr_{12}[n];\ P_2\{\phi_{22}[n] + f_{22}(\phi_{21}[n])\} \\ &= P_1\{1 - \phi_{12}[n] + f_{11}(\phi_{12}[n])\} \end{aligned} \quad (4)$$

The above mapping gives the evolution of a 2:2 locking in which the firing order does not change for all time. The periodicity constraints can be obtained by allowing the $\phi_{ij}[n]$ to go to their steady state values ϕ_{ij}*. The stability of a fixed point of the mapping, corresponding to a periodic pattern in the corresponding two-neuron circuit can be determined by assuming a perturbation from the steady state such that $\phi_{ij}[n]=\phi_{ij}^*+\Delta\phi_{ij}[n]$ (Dror et al. 1999; Oprisan and Canavier 2001). By linearizing the PRC we get $f_{ki}(\phi_{ij}[n])=f_{ki}(\phi_{ij}^*)+m_{kij}\Delta\phi_{ij}[n]$, where m_{kij} is the slope $f'_{ki}(\phi_{ij}^*)$ for the kth order resetting of neuron i when it receives input j. The linearized system, after canceling all of the steady state components and rearranging, is

$$\Delta\phi_{11}[n] = (P_2/P_1)(m_{122}-1)\Delta\phi_{22}[n-1] - m_{212}\Delta\phi_{12}[n-1];$$

$$\Delta\phi_{21}[n] = (P_2/P_1)(m_{111}-1)\Delta\phi_{11}[n] - m_{222}\Delta\phi_{22}[n-1];$$

$$\Delta\phi_{12}[n] = (P_2/P_1)(m_{121}-1)\Delta\phi_{21}[n] - m_{211}\Delta\phi_{11}[n];$$

$$\Delta\phi_{22}[n] = (P_2/P_1)(m_{112}-1)\Delta\phi_{12}[n] - m_{221}\Delta\phi_{21}[n];$$

A stable 2P mode is predicted if the roots of the following characteristic equation of the linearized system have an absolute value less than 1: $0=\lambda^2+\lambda\ [-(1-m_{111})(1-m_{112})$

$(1-m_{121})(1-m_{122}) + m_{211}(1-m_{112})(1-m_{122}) + m_{221}(1-m_{111})(1-m_{122}) + m_{212}(1-m_{111})(1-m_{121}) + m_{222}(1-m_{112})(1-m_{121}) - m_{211}m_{212} - m_{221}m_{222}] + m_{211}m_{212}m_{221}m_{222}$.

A similar analysis can be conducted for the 2:2 locking in which the firing order changes every cycle. The assumed firing pattern for a 2:2 locking in which the firing order changes every cycle is given in Fig. 3(b). The definitions of ts and tr must be slightly modified. For example, ts_{11} and ts_{21} are defined the same way as the stimulus intervals above, but there is no second order resetting in these intervals because the previous intervals, tr_{12} and tr_{22} respectively, did not contain any synaptic inputs. The intervals ts_{12} and ts_{22} are defined as the interval between the first and second inputs within a single cycle, obtained by subtracting the phase at the first input from that of the second, then adding the first order reset due to the first input, and multiplying by the intrinsic period. The intervals tr_{11} and tr_{21} are defined as above, but the intervals tr_{12} and tr_{22} are obtained by adding the second order resetting due to both inputs in the previous cycle to the intrinsic period, since no input is received in those intervals. The assumed firing pattern implies that the following intervals must be equal by definition: $ts_{11}=tr_{21}$, $ts_{12}=tr_{22}$, $ts_{21}=tr_{11}$, $ts_{22}=tr_{12}$. Note that ts_{11} is not qualitatively equal to ts_{12} because the ts_{11} interval begins with a spike in neuron 1 and ts_{12} does not. No intervals are qualitatively equal to each other in this firing pattern, hence there is no symmetry in the solution structure and a 1:1 locking cannot be a solution to this firing pattern.

Combining the expressions for intervals known to be equal in a steady state mode yields the following mapping

$$\begin{aligned} ts_{11} &= tr_{21}; P_1\{\phi_{11}[n]\} \\ &= P_2\{1-\phi_{22}[n-1]+f_{12}(\phi_{22}[n-1])\} \end{aligned} \quad (5)$$

$$\begin{aligned} ts_{12} &= tr_{22}; P_1\{\phi_{12}[n]-\phi_{11}[n]+f_{11}(\phi_{11}[n])\} \\ &= P_2\{1+f_{22}(\phi_{21}[n-1])+f_{22}(\phi_{22}[n-1])\} \end{aligned} \quad (6)$$

$$ts_{21} = tr_{11}; P_2\{\phi_{21}[n]\} = P_1\{1-\phi_{12}[n]+f_{11}(\phi_{12}[n])\} \quad (7)$$

$$\begin{aligned} ts_{22} &= tr_{12}; P_2\{\phi_{22}[n]-\phi_{21}[n]+f_{12}(\phi_{21}[n])\} \\ &= P_1\{1+f_{21}(\phi_{11}[n])+f_{21}(\phi_{12}[n])\} \end{aligned} \quad (8)$$

The coupled map above completely describes the evolution in time of a 2:2 locking in which the firing order changes every cycle. In order to find the periodicity criteria, simply set all $\phi_{ij}[n]$ to their steady state value ϕ_{ij}^* as before. The next section describes how to find the set of ϕ_{ij}^* that satisfy Eqs. (5–8) above. The stability of such a mode can be determined using a perturbation analysis and linearizing as before. In this case we obtain the following linearized system:

$$\Delta\phi_{11}[n] = (P_2/P_1)(m_{122}-1)\Delta\phi_{22}[n-1];$$

$$\Delta\phi_{21}[n] = (P_1/P_2)(m_{112}-1)\Delta\phi_{12}[n];$$

$$\begin{aligned} \Delta\phi_{12}[n] &= (1-m_{111})\Delta\phi_{11}[n] + (P_2/P_1)m_{221}\Delta\phi_{21}[n-1] \\ &\quad +(P_2/P_1)m_{222}\Delta\phi_{22}[n-1]; \end{aligned}$$

$$\begin{aligned} \Delta\phi_{22}[n] &= (1-m_{121})\Delta\phi_{21}[n] + (P_1/P_2)m_{211}\Delta\phi_{11}[n] \\ &\quad +(P_1/P_2)m_{212}\Delta\phi_{12}[n]; \end{aligned}$$

A stable leapfrog 2P mode is predicted if the roots of the following characteristic equation of the linearized system have an absolute value less than 1:0=$\lambda^2-\lambda[m_{221}(m_{112}-1)+m_{211}(m_{122}-1) + \{m_{212} + (1-m_{121})(m_{112}-1)\}\{m_{222}+(1-m_{111})(m_{122}-1)\}] + m_{211}m_{221}(1-m_{112})(1-m_{122})$. Note that the stability results for the two 2:2 modes are different, but if second order resetting is ignored, they both reduce to $\lambda=(1-m_{111})(1-m_{112})(1-m_{121})(1-m_{122})$.

2.5 Finding the sets of phases that satisfy the periodicity criteria

This is a nontrivial problem, and two different methods were attempted. There are four different criteria [the steady state version of Eqs. (1–4) or (5–8)] that need to be satisfied exactly in the four-dimensional space (ϕ_{11}, ϕ_{12}, ϕ_{21}, ϕ_{22}) of the phases at which inputs are received. One approach utilized error minimization (described in Appendix I), and the other was a graphical method (details in Appendix II). The graphical method searches for intersections between two curves in a plane that was structured so that all points in one curve satisfied three of the four criteria, and all points on the other curve satisfied a different set of three criteria.

Figure 4(a) shows the graphical method for the 2:2 lockings in which firing order is preserved. On the blue curve, the criteria $ts_{11}=tr_{22}$, $ts_{12}=tr_{21}$, and $ts_{21}=tr_{11}$ are satisfied, whereas on the red curve, the criteria $ts_{11}=tr_{22}$, $ts_{12}=tr_{21}$, and $ts_{22}=tr_{12}$ are satisfied. The axes of the plot are structured so that at the intersection of the curves all four criteria are met, so the red curve shows we plot ts_{11} and tr_{21}. The graphical method for these modes also predicts all 1P modes as points on the 45° diagonal. The point at $ts_{11}=ts_{12}=2.594$ ms corresponds to a 1P mode with $ts_{21}=ts_{22}=8.691$ ms that was predicted to be unstable and was not observed. Equations (1–4) are symmetrical in that the indices corresponding to the jth input in ϕ_{ij} can be

renumbered so that the first and second inputs are switched and still be correct. Thus the red curve could be generated simply by switching the x and y points in the blue curve.

Figure 4(b) is a magnification of the area in the lower left hand corner of Fig. 4(a). Another intersection on the 45° diagonal at $ts_{11}=ts_{12}=0.223$ ms corresponds to a near synchronous mode with $ts_{21}=ts_{22}=10.132$ ms that was also predicted to be unstable and was not observed. Due to the above-mentioned symmetry, the 2P modes appear twice at (ts_{11}, ts_{12}) and (ts_{12}, ts_{11}). The predicted and observed values for the short intervals ts_{11} and ts_{12} were 0.601 and 0.048 ms and 0.497 and 0.069 respectively, and for the long intervals ts_{21} and ts_{22} were 10.049 and 10.052 ms and 10.067 and 10.101 ms, respectively. Hence the graphical method produces reasonably accurate predictions.

The graphical method was also utilized for the 2:2 locking in which the firing order changes every cycle (see Fig. 5). We sometimes refer to this mode as a leapfrog mode. In a leapfrog mode, one neuron that fires after its partner on one cycle, fires before it on the next, in an analogy to a childhood game in which one child is behind a second child, then leaps over the second child in a froglike manner to achieve a position ahead of the second child. On the red curve in Fig. 5, the criteria $ts_{11}=tr_{21}$, $ts_{21}=tr_{11}$, and $ts_{22}=tr_{12}$ are satisfied, whereas on the blue curve, the criteria $ts_{11}=tr_{21}$ $ts_{12}=tr_{22}$, and $ts_{21}=tr_{11}$ are satisfied. There is no guarantee that these criteria will be satisfied at any value of ts_{12}, and the shortness of the blue curve compared to the red shows that its particular criteria can only be satisfied in a narrow range of values. The axes of the plot are structured so that at the intersection of the curves all four criteria are met. This intersection point is

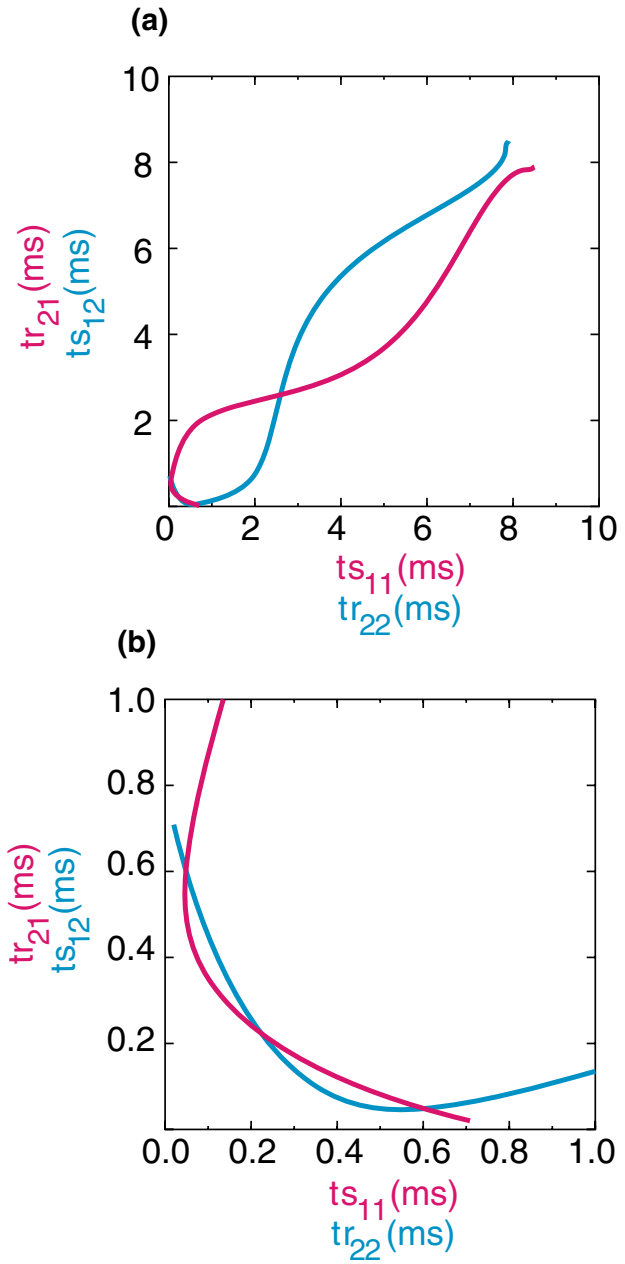

Fig. 4 Graphical prediction of 2:2 locking with firing order preserved. The parameter values were $g_{syn}=0.35$ mS/cm^2 and $\tau_{syn}=1$ ms, $I_{app}=2.0$ μA/cm^2 and $\varepsilon=0.07$ μA/cm^2. (**a**) The intersections of the two curves indicate intervals at which all four periodicity criteria are satisfied. A different set of three of the four criteria are satisfied on each curve. (**b**) Magnification of the region around the origin in panel (**a**). This graphical method is symmetric because the existence criteria are symmetric with respect to switching the indices indicating inputs 1 and 2

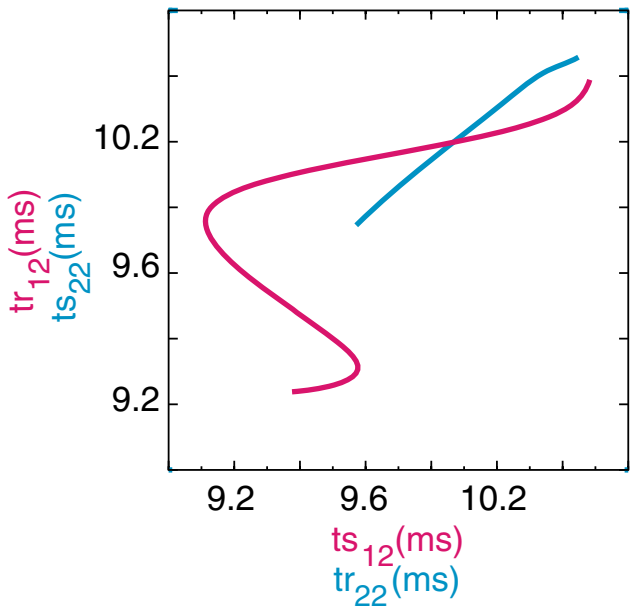

Fig. 5 Graphical prediction of 2:2 locking with firing order not preserved. The parameter values were $g_{syn}=0.35$ mS/cm^2, $\tau_{syn}=1$ ms, $I_{app}=2.0$ μA/cm^2 and $\varepsilon=0.03$ μA/cm^2. A different set of three of the four periodicity criteria for this mode are satisfied on each curve. The axes of the plot are structured so that at the intersection of the curves all four criteria are met

$ts_{12}=tr_{22}=9.867$ ms and $ts_{22}=tr_{12}=9.998$ ms, and the actually observed values for this example were 9.899 and 9.996 ms, respectively. One can calculate that at the intersection $ts_{11}=tr_{21}=0.760$ ms and $ts_{21}=tr_{11}=0.213$ ms. The actually observed values were 0.706 and 0.206 ms respectively. Note that the assumptions in Fig. 3(b) do not apply to 1:1 modes, since ts_{11} and ts_{12} are not defined in the same way, hence each leapfrog mode is found only once, and this graphical method does not find 1:1 lockings.

2.6 Weak coupling method

The weak coupling methodology outlined in Rinzel and Ermentrout (1998) was followed with one exception. Instead of using the adjoint as the infinitessimal PRC (iPRC), the iPRC with respect to a conductance pulse was used in order to get the results in the appropriate units, since the synaptic coupling in this model is formulated in terms of the synaptic conductance. However, see Netoff et al. (2005a) for an alternate approach in which the iPRC with respect to a current pulse is convolved with the synaptic current rather than the conductance. Figure 6(a) shows the synaptic conductance waveform (black) and the iPRC (red curve) evoked by a square pulse in synaptic conductance. The phase resetting is divided by the width of the pulse and converges to the red curve in Fig. 6(a) as the width of the pulse goes to zero. Somewhat surprisingly, there is a second order component to the iPRC (blue curve). The limit cycle is far from the saddle node bifurcation that underlies the Type I excitability (Ermentrout 1996) of this model, and even a small perturbation causes the trajectory to deviate from the limit cycle enough to produce a noticeable alteration in the duration of the cycle following the one containing the perturbation. Since the definition of weak coupling is that the strength of the attraction to the limit cycle is strong compared to the strength of the coupling, the presence of second order resetting does not bode well for the success of the application of weak coupling theory to this oscillator. The assumptions of weak coupling and mild heterogeneity require that there be only small differences between the network frequency and the intrinsic frequency of each component oscillator.

An example prediction using the methods of weak coupling is given in Fig. 6(b). For small values of $H(\phi)$, the coupling function $H(\phi)$ approximates the change in frequency caused by the coupling at an average phase difference of ϕ. The $H(\phi)$ functions were generated as follows:

$$H_1(\phi) = T_1 \Delta \sum_{i=1}^{N} P_1(\theta_i - \phi)\, R_1(\theta_i) \text{ and}$$
$$H_2(\phi) = T_2 \Delta \sum_{i=1}^{N} P_2(\theta_i + \phi)\, R_2(\theta_i)$$

where the T_i are the intrinsic periods, Δ is the width of each P_i pulse (0.01) in units of phase, N is 100, the θ_i range from 0 to 0.99, P_i is the sampled conductance waveform, and R_i is the sampled infinitesimal PRC. The iPRC shown uses the opposite sign convention than the one typically used in the weak coupling method. $H(\phi)$ theoretically approximates the first order PRC [red trace in Fig. 2(b)] that we generated numerically using the same conductance perturbation shown in Fig. 6(a) (black trace). The estimated change in the period is $1-H(\phi)$, so the estimated new frequency is $1/(1-H(\phi))$ and at small values of $H(\phi)$, this frequency is closely approximated by $1+H(\phi)$. Therefore $H(\phi)$ approximates the change of frequency for one oscillator, and $G(\phi)$ represents the differential effect on the frequency of the two oscillators $(H_1(\phi)-H_2(-\phi))$ and intersects with the line given by the normalized intrinsic frequency difference $\omega_2-\omega_1$ at a phase-locked mode. The solid curve was generated for a synaptic conductance of 0.25 mS/cm^2 and intersects the dashed line at four points. Only two points have a negative slope, making them stable using weak coupling theory. The first stable point is near a phase of zero and

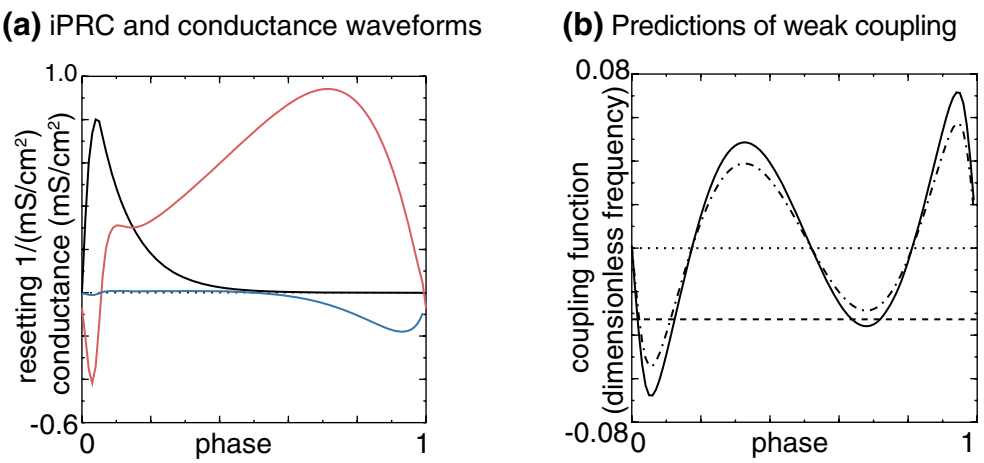

Fig. 6 Application of weak coupling theory. (**a**) Conductance waveform (*black*), first order iPRC (*red*), second order iPRC (*blue*). Wang and Buzsáki model with $I_{app}=2$ μA/cm^2 and $\tau=1$ ms. (**b**) Coupling function $G(\phi)$ at $\varepsilon=0.045$ μA/cm^2 with $g_{syn}=0.25$ mS/cm^2 (*solid black curve*) and with $g_{syn}=0.20$ mS/cm^2 (*dot-dashed black curve*). The *dotted line* indicates 0 and the *dashed line* indicates the normalized frequency difference between the oscillators

corresponds to near synchrony whereas the second is near a phase of 0.5 and corresponds to near anti-synchrony. Decreasing the conductance to 0.20 mS/cm^2 (dot-dashed curve) simply scales the coupling function, such that the intersection near anti-phase no longer exists.

3 Results

3.1 PRC methods successfully predict 2:2 as well as 1:1 lockings in the 2 neuron circuit

We examined the parameter space of the two neuron circuits composed of Wang and Buzsáki model neurons in order to determine if the methods developed herein for predicting observed patterns based solely on the PRC were applicable to this system. In order to predict a pattern, it must meet the periodicity criteria for existence described in the methods, and stability criterion described must also be met because only stable patterns will be observed in practice. Figure 7(a) shows the 1:1 and 2:2 patterns predicted by the PRC methods as the synaptic conductance g_{syn} and the heterogeneity parameter ε are varied. Recall that the method for predicting the 2P modes in which the firing order remains constant with the two neurons firing in the same order on each cycle also predicts all 1:1 lockings. Figure 7(a) shows that near antiphase 1:1 (black plus signs) is often predicted at low heterogeneity. At low values of g_{syn} near synchronous 1:1 (blue circles) is also predicted at low heterogeneity. However, as g_{syn} is increased, the phase resetting increases at each phase, and more heterogeneity is required to support near synchronous firing. At some values of g_{syn}, a leapfrog 2:2 mode (green circles), or one in which the firing order switches, emerges at low heterogeneity and is bistable with near antiphase. As heterogeneity is increased, a 2:2 mode with a constant firing order (red circles) sometimes appears before the 1:1 near synchronous mode is reached. The qualitative agreement between theory [Fig. 7(a)] and observation [Fig. 7(b)] is quite good, with some errors at the borders between regions. The gray circles in Fig. 7(b) indicate complex lockings, which sometimes are bistable with antiphase, and are discussed in more detail below. The observation of these modes does not indicate a failure of the method, because we do not explicitly predict or rule out any modes except the 1:1 and 2:2 modes that the graphical PRC methods described herein detect. The complex lockings are not indicated on subsequent qualitative summaries of modes predicted and observed.

In order to determine whether the strong coupling method is an advance over the weak coupling method for this particular example, the weak coupling methodology (Ermentrout 2002; Rinzel and Ermentrout 1998) was applied to the same networks. Figure 7(c) shows the predictions based on the assumptions of weak coupling and mild heterogeneity. Since this methodology assumes 1:1 locking, there are no red or green circles indicating any 2P modes. The predictions of near synchrony and near antiphase are reasonable at weak values of conductance and small values of ε for mild heterogeneity, as expected. The weak coupling method captures the loss of the near synchronous mode (blue circles) as heterogeneity is increased and that larger conductances support near synchrony at larger values of heterogeneity. The weak coupling method fails to predict the loss of the near synchronous mode at low values of heterogeneity for higher conductance values, whereas the strong coupling method described above captured this trend quite nicely. The weak coupling method somewhat overestimates the

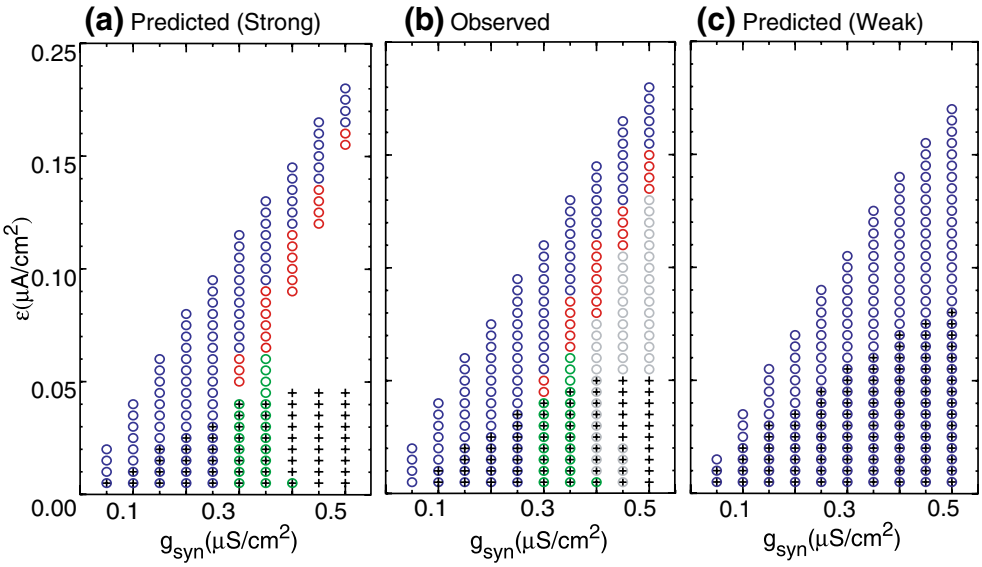

Fig. 7 Qualitative prediction of the firing pattern as g_{syn} is varied. Patterns include antiphase locking (*plus sign*), near synchronous 1:1 locking (*blue circles*), near synchronous alternating 2P locking (*red circles*), and near synchronous 2P leapfrog locking (*green circles*). If more than one symbol is plotted, bistability is indicated. The parameter values were I_{app}=2.0 μA/cm^2 and τ_{syn}=1 ms, and ε is also varied. (**a**) Predicted patterns (strong coupling method). (**b**) Observed patterns. The *gray circles* indicate complex lockings that cannot be predicted by the graphical method. (**c**) Predicted patterns (weak coupling method)

range of stability and existence for the antiphase solution (pluses). These failures are in no way an indictment of the weak coupling method, they simply show that the underlying assumptions are not met in this example. The strong coupling method applies because it does not rely on the additional assumptions required by the weak coupling method.

Figure 8 illustrates the predictive power of the methods in heterogenous networks as the applied current i_{app} is varied. Figure 8(a) shows that near antiphase 1:1 (black plus signs) is often predicted at low heterogeneity, and that as heterogeneity is increased, near synchronous 1:1 (blue circles) emerges. As in Fig. 7, some values of I_{app} support a leapfrog 2:2 mode (green circles) at low heterogenity which is bistable with near antiphase. The same trend is observed as in Fig. 7 that as heterogeneity is increased, the leapfrog mode is replaced by a 2:2 mode with a constant firing order (red circles), then by a 1:1 near synchronous mode (blue circles). Figure 8(b) shows the patterns that were observed by running simulations of the two neuron circuit. The firing pattern predicted across the parameter space again matches the observed patterns fairly well. In the gaps where no mode was observed, complex lockings as well as asynchrony could be observed [not shown in Fig. 8(a and b), but see Fig. 8(c and d) described in the next section]. These gaps are often found between near antiphase and near 1:1 synchronous lockings. At the borders where the firing pattern changes, the absolute value of the largest root λ can be close to one, making the prediction susceptible to error, or else the intersection of the branches described in the graphical method is close to disappearing, also making the prediction susceptible to error.

Figure 9 shows the quantitative agreement of the predicted firing intervals with the observed ones for the column in Fig. 8(a and b) labeled I_{app}=2.0 μA/cm^2. The predictions are open circles whereas the plus signs

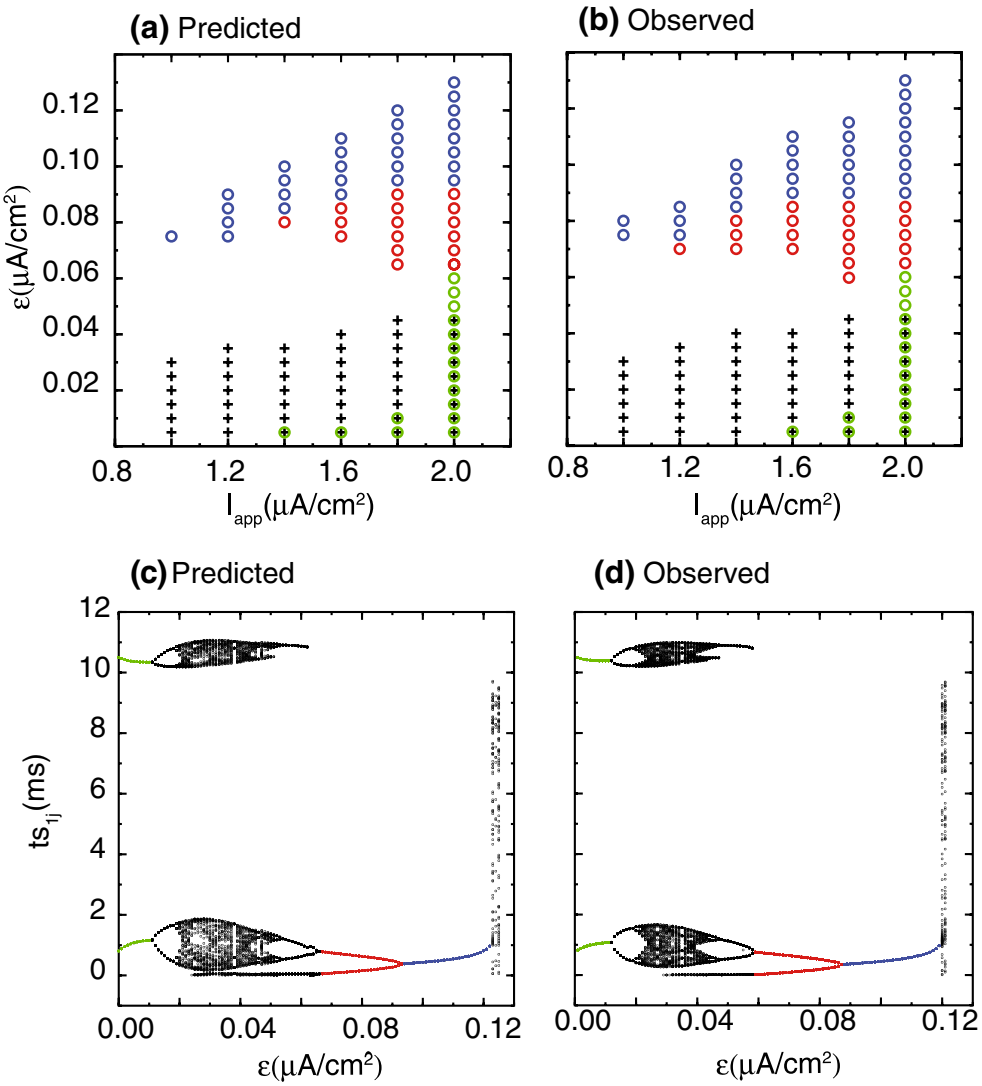

Fig. 8 Qualitative prediction of the firing pattern as I_{app} is varied. Patterns include antiphase locking (*plus sign*), near synchronous 1:1 locking (*blue circles*), near synchronous alternating 2P locking (*red circles*), and near synchronous 2P leapfrog locking (*green circles*). If more than one symbol is plotted, bistability is indicated. The parameter values were g_{syn}=0.35 mS/cm^2 and τ_{syn}=1 ms, and ε is also varied. (**a**) Predicted patterns. (**b**) Observed patterns. (**c** and **d**) Bifurcation diagram. (**c**) The predicted stimulus interval values of the faster neuron (ts_{1j}) are shown at g_{syn}=0.35 mS/cm^2, τ_{syn}=1 ms, I_{app}=1.8 mA/cm^2 as ε is varied. (**d**) The observed values at the same parameter values used in Fig. 8(c)

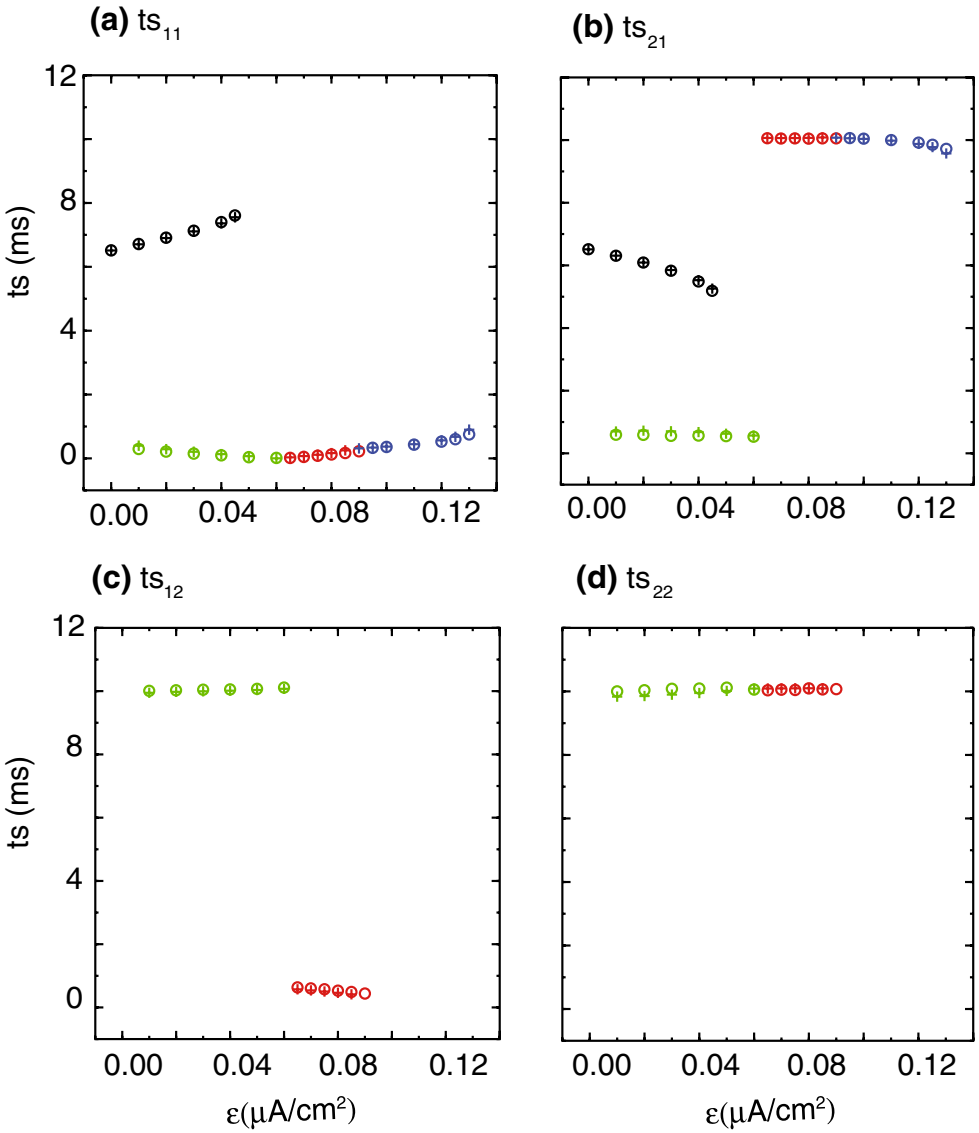

Fig. 9 Quantitative prediction of the firing pattern. The predicted stimulus times (*open circles*) are compared with the observed stimulus times (*plus sign*) at each value of ε for the column in Fig. 8(a and b) labeled I_{app}=2.0 μA/cm^2. The other parameters remain g_{syn}=0.35 mS/cm^2 and τ_{syn}=1 msas shown in Fig. 8. Antiphase (*black*), near synchrony (*blue*), alternating 2P (*red*), leapfrog 2P (*green*). The ts_{12} and ts_{22} for antiphase and near synchronous 1P are not shown in figure because they are the same as ts_{11} and ts_{21}. The quantitative fit to the firing intervals is fairly accurate

are observed values. Figure 9(a and b) shows ts_{11} and ts_{21}, respectively, which in a 1:1 mode completely define the firing pattern. For the antiphase mode (black symbols) the two intervals are close to equal, whereas for the nearly synchronous mode (blue symbols), one interval is much shorter than the other. In the 2:2 mode in which the firing order is preserved (red symbols), both stimulus intervals in one neuron are short (a, c) whereas they are long in the other (b, d). In contrast, for the leapfrog 2:2 mode (green symbols) each neuron has a long interval and a short one. The quantitative agreement is quite reasonable.

3.2 Other solutions, such as asynchrony and complex lockings

Very complex *n*:*n* lockings [see Fig. 8(c and d)], in which *n* could be as large as infinity, were observed at the ε values in the gap between the near antiphase and near synchronous 1:1 and 2:2 lockings. Although we could not predict the stability of these modes *a priori*, the emulator was able to produce very similar output. Figure 8(c) (bifurcation diagram) shows the predicted stimulus interval values of the faster neuron (ts_{1j}) at parameter values g_{syn}=0.35 mS/cm^2, τ_{syn}=1 ms, I_{app}=1.8 μA/cm^2 using the emulator algorithm. The corresponding observed values obtained from simulations of the two neuron network for the parameter values used in Fig. 8(c) are shown in Fig. 8(d). The example shown corresponds to the vertical column in Fig. 8(b) at I_{app}=1.8 μA/cm^2. Note the stimulus interval definitions differ depending on the mode (leapfrog or constant firing order) in which the neurons fire. The value of ts_{1j} was calculated as the time interval between an action potential in slower neuron and the action potential immediately preceding it, regardless of whether the preceding action

potential occurred in neuron 1 or 2. This definition corresponds to ts_{ij} in both Fig. 3(a and b), and used consistently in Fig. 8(c and d). The branches corresponding to leapfrog 2P in which the firing order changes are shown in green, to 2P with constant firing order in red, and to 1:1 near synchronous locking in blue. The remaining black points indicate complex lockings or asynchrony. The complex lockings do not fill the entire space of possible intervals, but rather form clusters, whereas asynchrony does not cluster. The complex lockings were often bistable with the antiphase mode, which is not shown in this figure. The complex lockings shown here are of the leapfrog variety, since there are both short and long intervals in neuron 1 (see also Fig. 9). Above the values for which 1:1 near synchronous modes were observed, only asynchrony could be found at 0.12.

3.3 Limits of the method with respect to the time constant to period ratio

The method assumes that the effects of one presynaptic action potential have dissipated by the time that the next presynaptic action potential occurs. As the ratio of the synaptic time constant to the network period (T_N) increases this becomes less accurate. One problem is that at high τ_{syn}/T_N ratios the synaptic activation never falls to zero between presynaptic inputs, so there is a tonic component that is on all the time, causing the effective intrinsic frequency to be slower than that used to generate the PRC. Figure 10(a and b) shows the qualitative degradation of the correspondence between the predicted modes [Fig. 10 (a)] and the observed modes [Fig. 10(b)] as τ_{syn} is increased at a constant value of I_{app}=2.0 μA/cm^2 and g_{syn}=0.2 mS/cm^2.

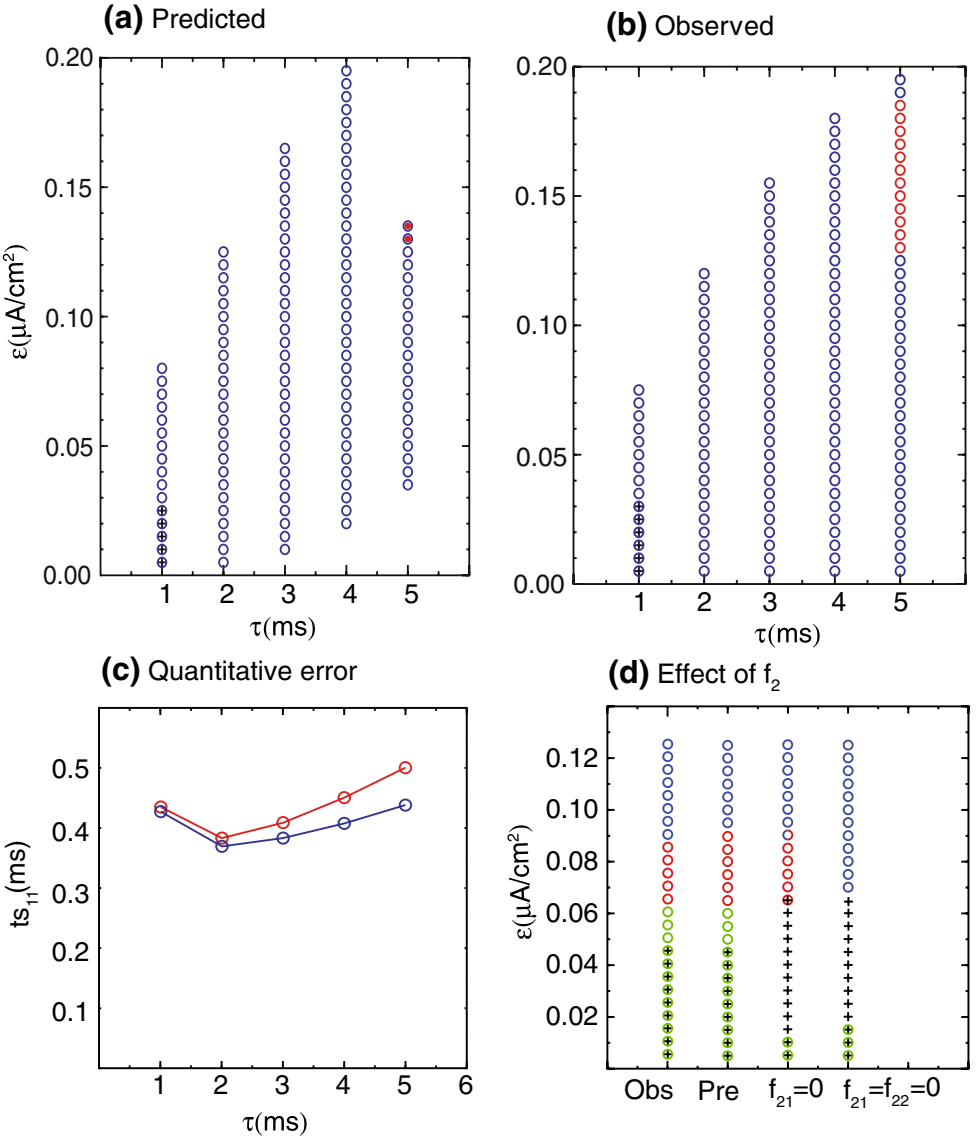

Fig. 10 Degradation of predictions as the time constant is increased or the second order resetting is neglected. (**a**, **b** and **c**) Effect of increased time constant: The parameter values were g_{syn}=0.2 mS/cm^2 and I_{app}=2 μA/cm^2, and ε is varied. (**a**) Predicted modes. (**b**) Observed modes. (**c**) The predicted ts_{11} interval (*blue*) is plotted versus observed ts_{11} (*red*) as τ_{syn} is varied at ε=0.07 μA/cm^2. (**d**) Prediction without second order resetting. The parameter values are g_{syn}= 0.35 mS/cm^2, τ_{syn}=1 ms, I_{app}= 2 mA/cm^2. The first column (*Obs*) shows the observed modes, the second column (*Pre*) shows the predicted modes when the second order resetting of both neurons is included, the third shows the prediction when the second order resetting of faster neuron is zero (f_{21}=0), and the fourth (f_{21}=f_{22}=0) shows the prediction when the second order resetting of both neurons is zero. The qualitative patterns include near synchronous 1:1 locking (*blue circles*), near synchronous alternating 2P locking (*red circles*), and near synchronous 2P leapfrog locking (*green circles*). The *blue circles filled with red* indicate a prediction of bistability between two modes

The qualitative prediction is quite accurate at $\tau_{syn} \leq 3$ ms, with only an occasional error at the border of the parameter space in which a mode is expressed. At higher values of τ_{syn} there are many qualitative errors. These qualitative errors arise from an accumulation of quantitative errors in the prediction [see Fig. 10(c)] as τ_{syn} is increased at a constant value of ε. The discrepancy between the predicted and observed ts_{11} is small for $\tau_{syn}=1$ and 2 but diverges sharply for larger values. The main reason for the divergence is that the second order resetting due to one input, as measured in Fig. 2(a), is not complete by the time the next input is received in the circuit. The network period for a near synchronous mode at the parameter sets shown in Fig. 10 is approximately 10 ms, so at a ratio τ_{syn}/T_N of less than or equal to 0.2 performance is satisfactory. As that ratio increases the prediction becomes less accurate.

3.4 Importance of second order resetting

Figure 10(d) shows the result of omitting second order resetting from the prediction method for the column in Fig. 8(a and b) labeled $I_{app}=2.0$ μA/cm^2. It is not possible to selectively remove the effect of second order resetting from the model simulations, but it is simple to remove the second order terms from the prediction method. The far left column shows the observations, and the second column from the left shows the predictions including the effects of second order resetting. The only error is that at $\varepsilon=0.09$ the alternating 2P mode is predicted instead of 1:1 near synchronous mode. However, if the second order resetting for the faster neuron, which in this case is neuron 1, is omitted, then most of the leapfrog modes are missed, and the near antiphase mode is incorrectly predicted instead in four instances. The 2:2 mode with a constant firing order is still predicted correctly, because neuron 1 fires first and does not receive any significant second order resetting in that mode. Note that at $\varepsilon=0.09$ a spurious modes 2:2 mode is predicted to be bistable with the 1:1 mode. However, if second order resetting for both neurons is ignored, the 2:2 modes with constant firing order are no longer correctly predicted, and in most cases 1:1 near synchrony is incorrectly predicted instead. The leapfrog modes are also not predicted here, with an incorrect prediction of 1:1 near antiphase again in some cases. Interestingly, the failures of the method described in Fig. 10 when second order resetting is ignored are caused by changes in the criteria for existence, rather than stability. Without taking second order resetting into account, some modes cease to exist, and others appear as spurious intersections in the graphical method described in Section 2.

3.5 Firing order is not preserved even in identical oscillators

Can the firing order also alternate for a pair of identical neurons? Yes, an example of this type of firing was observed in Fig. 11(a) at $g_{syn}=0.35$ mS/cm^2, $I_{app}=2.0$ μA/cm^2, $\tau_{syn}=1$ and $\varepsilon=0$. Both the emulator and the method based on existence and stability criteria correctly predicted the leapfrog mode. In the full system of differential equations, as in physiological neurons, the contribution of second order resetting cannot be set to zero. However, in both prediction methods this is indeed possible, and both predict synchrony instead of the leapfrog mode if second order resetting is ignored. Similarly, an instance of a convergence to synchrony in which the firing order alternates was observed in Fig. 11(b) at $g_{syn}=0.25$ mS/cm^2, $I_{app}=2$ $\tau_{syn}=1$

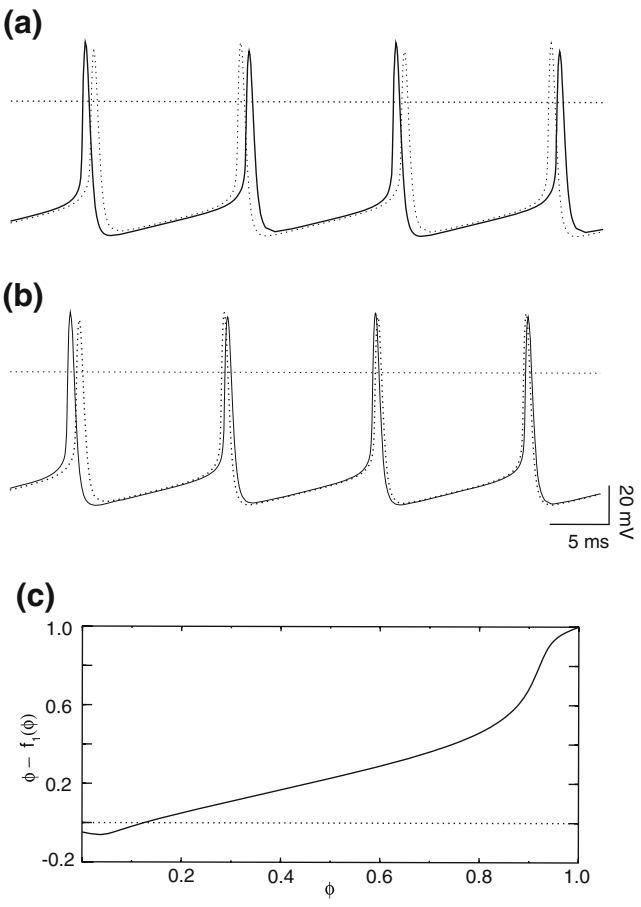

Fig. 11 Homogeneity does not guarantee that the firing order is preserved. (**a**) Leapfrog 2:2 locking of identical oscillators. The parameters were $g_{syn}=0.35$ mS/cm^2, $I_{app}=2.0$ μA/cm^2, $\tau_{syn}=1$ and $\varepsilon=0$. (**b**) Convergence to synchrony of identical oscillators in which the firing order is not preserved. The parameters were $g_{syn}=0.25$ mS/cm^2, $I_{app}=2.0$ μA/cm^2, $\tau_{syn}=1$ and $\varepsilon=0$. (**c**) The new phase versus old phase function generated at $g_{syn}=0.35$ mS/cm^2 and $\tau_{syn}=1$ ms, and $I_{app}=2.0$ μA/cm^2 ($\varepsilon=0.0$ μA/cm^2)

and ε=0. Neither heterogeneity nor second order resetting are required in order to observe switching of the firing mode, even though both can enhance the chances of observing such a mode. A new phase versus old phase function that is not monotonically increasing, as shown in Fig. 11(c) for the parameter values in Fig. 11(b) can contribute, as explained in Section 4.

3.6 The firing order is also not preserved in larger networks

In order to determine whether stable 2:2 modes can be seen in larger networks, networks consisting of ten neurons (N=10) with all to all connections were examined. In order to compare the results with those of the two neuron network, the values of I_{app} and τ_{syn} were held constant at 2.0 μA/cm^2 and 1 ms as in Fig. 7. The values of the individual synaptic conductances were scaled to $g_{syn}/(N-1)$ to keep the total conductance in the range given by Bartos et al. (2001), and the values of applied current for the each of the ten neurons were evenly distributed over the interval $[I_{app}-\varepsilon, I_{app}+\varepsilon]$. Stable 2:2 leapfrog modes were observed, such as the one in Fig. 12(a). Here the neuron indicated in orange fires first and the neuron indicated in blue fires last in the first cycle shown, but reverse these roles in the second cycle shown. The difference between the firing times of the leading and lagging neuron on each cycle is about 17% of the cycle period. The raster plot in Fig. 12(b) shows that the pattern repeats every other cycle.

At low heterogeneity, Fig. 12(c) shows that the dependence of the ten neuron network on heterogeneity as implemented by ε and on g_{syn} is qualitatively similar to that for the two neuron network shown in Fig. 7(b). As g_{syn} is increased, first 1:1 lockings with constant firing order are observed (blue circles), then the 2:2 leapfrog modes (green circles) in which the firing order alternates every other cycle, and finally only anti-phase (black plus signs) can be observed. Just as in the two neuron network, the antiphase mode was often bistable with the near synchronous modes. In the 10 neuron circuit, the antiphase mode is exhibited by two clusters of five neurons. Interestingly, 2:2 antiphase modes in which the firing order within each cluster also alternates every other cycle were observed. The 2P

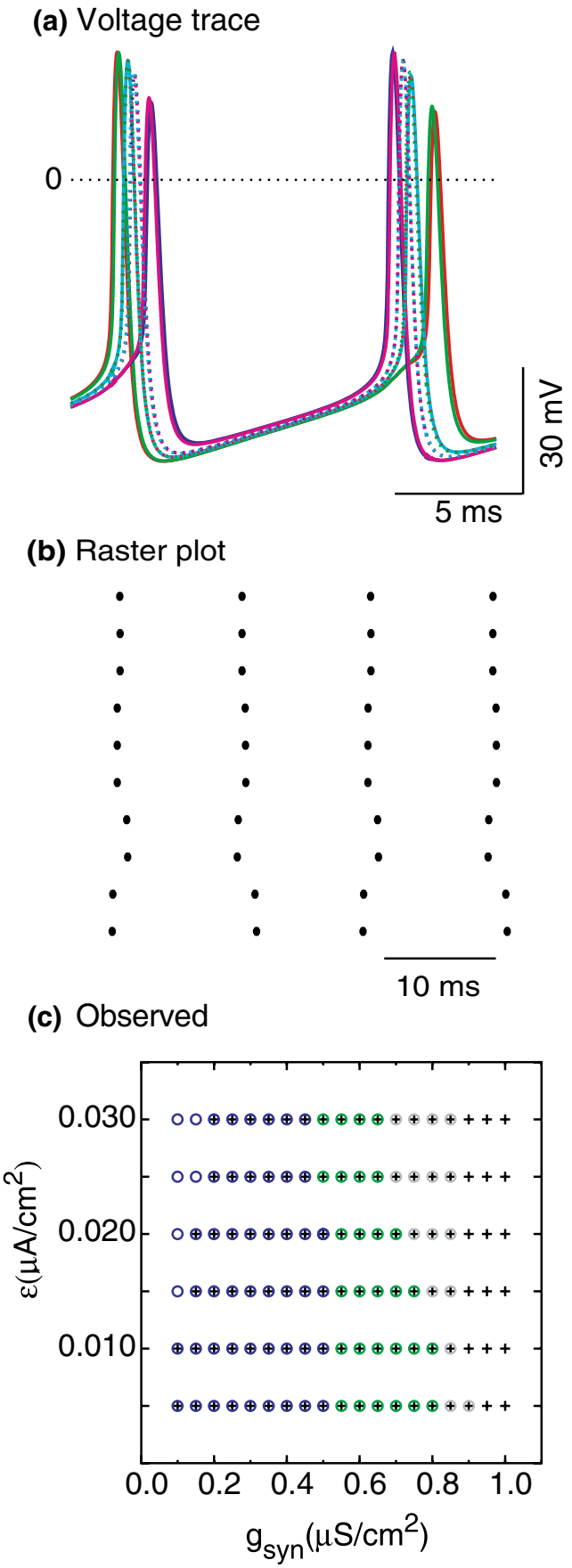

Fig. 12 2:2 modes in ten neuron network. (**a**) Membrane potential. Each different trace corresponds to the voltage waveform of a single neuron. The parameter values are g_{syn}=0.8/9 mS/cm^2, I_{app}=2.0 μA/cm^2, τ_{syn}=1 ms, and ε=0.01 μA/cm^2. The values of applied current (I_{stim}) for the each of the ten neurons were $I_{app}-\varepsilon+(n2\varepsilon)/9$, where n ranges from 0 to 9. (**b**) Raster plot. (**c**) Qualitative prediction of the firing pattern as g_{syn} is varied. The parameter values are I_{app}=2.0 μA/cm^2 and τ_{syn}=1 ms. The following modes are observed—1:1 near synchronous (*blue circles*), the 2:2 leapfrog modes (*green circles*), anti-phase (*black plus signs*) and complex lockings (*gray circles*)

near-synchronous modes occurs at somewhat larger values of synaptic conductance (0.55/9–0.8/9) compared to the two neuron network (0.3–0.4). Since g_{syn} for the individual synapses were scaled by $N-1$, the mapping from the smaller to the larger network is only exact for exact synchrony when each neuron receives $N-1$ synchronous inputs. Since exact synchrony does not occur in heterogenous networks, the actual inputs received are spread out in time and do not sum linearly. A smaller scale factor for the conductance would compress the parameter ranges observed in Fig. 12(c) and shift them to the right, improving the mapping between the two neuron and ten neuron networks. The comparison focused on small values of heterogeneity because at higher values, many modes arose with distinct clusters that did not map easily onto a two neuron network.

4 Discussion

4.1 Generality of the method

The PRC-based methods present in this study are very general. They require only two assumptions: (1) that the input that each neuron receives in the network closely resembles the input that was used to generate the PRC, and (2) that each neuron returns near its unperturbed limit cycle and the phase resetting due to the previous input is complete prior to receiving the next input. On the other hand, the head to head comparison with the weak coupling method shows that the additional assumptions required for weak coupling are not satisfied in physiologically realistic parameter regimes for the synaptic conductance (Bartos et al. 2001, 2002) used in this study and in a previous study (Skinner et al. 2005b).

In this study, it was assumed that the variation in postsynaptic conductance resulting from an action potential generated by the presynaptic neuron in isolation was the appropriate perturbation with which to generate the PRC. Although it is true that the action potential in the closed circuit network can have a smaller peak and a shallower after-hyperpolarization than in the free-running, open loop configuration, the perturbation in synaptic conductance is generally quite similar in the two configurations. In the case of circuits comprised of bursting neurons, the duration and intensity of a burst can vary greatly as a result of the network coupling, hence this assumption is potentially more problematic for networks of bursting neurons.

The assumption that the neuron return close to the limit cycle prior to the next input is quite likely to be fulfilled for Type I neural oscillators (Ermentrout 1996), because a perturbation in current generally does not perturb the limit cycle trajectory in a direction normal to the limit cycle (Oprisan and Canavier 2002). Since the action potential waveform is slightly changed, the perturbations in synaptic conductance (as opposed to current) do cause some small departure from the limit cycle. A necessary, but not sufficient condition for the return of the trajectory to the limit cycle by the time of the next input is that third order resetting be equal to zero. The reason it is not sufficient is that this condition still does not guarantee that the second order resetting is complete by the time the next input is received. The second order resetting is measured at the time of the second spike in the postsynaptic neuron after receiving a single input from the presynaptic neuron. The second order resetting at the time that the postsynaptic neuron returns to the same point on the limit cycle (that is, the same phase) at which the input was received is the relevant quantity, but is more difficult to measure. Inputs of long duration relative to the network period pose another potential problem with this assumption. As the synaptic time constant becomes longer relative to the network period, the performance of PRC methods breaks down [see Fig. 10(c)] since the coupling is no longer purely pulsatile. One possible resolution of this problem is to decompose the synaptic input into a tonic and phasic component, but the handling of the incomplete second order resetting under this scenario has yet to be resolved. Nevertheless, the method is accurate in situations where the synaptic time constant is one fifth or less than the network period, which encompasses many neural applications.

The ultimate goal for biological phase resetting theory is to understand synchronization in biological networks, but existing methods have limitations. The limitation of the weak coupling method is obviously the presumption of weak coupling, so that a synaptic coupling of significant duration can be decomposed into a train of short inputs whose effects are presumed to summate linearly. The limitation of the method presented in this paper is that inputs are presumed to exert their entire effect instantaneously. We have found a practical rule of thumb that prediction accuracy deteriorates when the network period is less than five times the synaptic time constant. This rule of thumb was borne out in a recent paper (Pervouchine et al. 2006), which used very similar PRC methods on reduced two-neuron networks. They showed how the hippocampal CA1 oriens lacunosum-moleculare (O-LM) cells can only synchronize at theta rhythm frequencies in the presence of inhibitory interneurons with short time constants (5 ms), similar to the model interneurons used in this study. The theta oscillation was 10 Hz (period=100 ms), and the slowest time constant, that of the OLM cells, was exactly one fifth of the period (20 ms). Their predictions were successfully tested in hybrid circuits created using biological and model neurons with the Dynamic Clamp. Another potential area of applicability for these methods is that of central pattern generating circuits (Kopell 1987), which

often have network frequencies on the order of one Hz or less, and in invertebrates which often contain only a few dozen neurons and can be further simplified by grouping functionally similar neurons (Marder and Calabrese 1996). Therefore, the intersection of strong coupling phase resetting theory with experimental data should prove to be fertile ground for scientific insight. The major limitation at this time is that the method needs to be scaled up to apply to larger networks receiving multiple inputs per cycle. Nevertheless, in our study, this method was able to provide insights into the activity of two neuron networks, and by analogy, into that of larger networks. This insight could not have been derived from the more widely applied methods based on the assumption of weak coupling.

4.2 Importance of second order resetting

Theoretically, there are two mechanisms by which second order resetting can occur. The most obvious is if the perturbation persists after a spike is elicited. The change in the first spike time is the first order resetting, but since the input is still on, it can also affect the timing of the second spike. The other way is if the perturbation finishes before the next cycle, but has moved the trajectory off the unperturbed limit cycle, and additional resetting occurs during the relaxation back to the limit cycle. Note that the second order resetting late in the cycle produces an advance in the model used in this study [see Fig. 2(b)]. This results because the inhibitory input is on during the action potential, which produces an action potential with a less depolarized peak, and a shallower hyperpolarization that subsequently requires less recovery time before the next action potential is produced. This is consistent with our understanding of phase resetting in Type I oscillators. They behave like integrators, so the application of an excitatory current advances the phase and that of an inhibitory current delays it. However, this result is true for infinitesimally small perturbations, and it is only true because the membrane potential is monotonically increasing during every portion of the cycle except the downstroke of action potential repolarization. An infinitesimal inhibitory perturbation applied during the downstroke actually advances the phase (Oprisan and Canavier 2002). The fact that an inhibitory IPSP with a time constant one tenth of the network period produces significant second order resetting, and that this resetting can have the opposite sign of first order resetting, is often ignored. Nonetheless, Preyer and Butera (2005) observed very similar second order resetting in response to an IPSP in invertebrate neurons, and Reyes and Fetz (1993) observed an analogous phenomenon for EPSPs in layer V cortical neurons. Second order resetting is likely to significantly impact near synchronous modes, since some neurons will always receive at least one input just prior to firing an action potential. This is evidenced by the degradation in predictive ability when second order resetting is ignored [see Fig. 10(d)]. Second order resetting can stabilize near synchronous modes. In neocortical pyramidal neurons, the transient outward potassium channels are responsible for second order resetting (Reyes and Fetz 1993), thus modulating the conductance of these channels could target synchronization properties.

4.3 Importance of the observed changes in firing order

Not only have we shown that firing order is not always preserved, but we have also shown that changes in firing order can lead to loss of synchrony in the following manner. If a stable near synchronous 1:1 locking is perturbed, then one neuron fires earlier and the other later compared to the stable locking, and the resultant phase resetting causes the neuron that fires earlier to increase its period and the one that fired later to decrease its period. This compensation tends to restore the locking. However, as the heterogeneity decreases or the conductance is increased, 1:1 locking is lost and replaced by 2:2 or more complex lockings [see Fig. 7(a and b)]. In a 2:2 leapfrog locking, there is an overcompensation causing the firing order to switch on every cycle. As the heterogeneity is further decreased or the conductance is increased, this overcompensation becomes so strong that it destabilizes the nearly synchronous 2:2 locking. An analogous phenomenon occurs in larger networks (see Fig. 12). This is a novel route by which synchrony is lost in mildly heterogenous networks (White et al. 1998).

The elegant work of Kuramoto and others exploring the onset of synchronization in populations of oscillators with smooth sinusoidal coupling (Strogatz 2000) using mean field formulations has been very influential because of its generality. However, this work assumes that the solutions have the simple form that the firing order of the individual oscillators within a synchronized cluster remains constant. Similarly, in one of the first papers on pulsatile coupling, Mirollo and Strogatz (1990) proved that all to all networks of identical oscillators coupled via pulsatile excitatory coupling would always synchronize under the following restrictive assumptions that guaranteed a constant firing order. They assumed that voltage increases monotonically as a smooth, concave down function of phase and is reset to zero at threshold. They also assumed that a perturbation in voltage instantaneously moved the trajectory to the phase associated with the new voltage. They ignored second order resetting, so in their scheme there was no way for one neuron in a two-neuron network to fire twice in a row without the partner firing in between. Goel and Ermentrout (2002) extended the results of Mirollo and Strogatz to networks of identical oscillators with all-to-all pulse

coupling, assuming only that the new phase versus old phase function is monotonically increasing, which guarantees that the firing order will be preserved during the approach to synchrony. The new phase versus old phase function is the mapping of the phase before a perturbation to the phase afterward by subtracting first order resetting from the phase. They also ignore second order resetting. Both heterogeneity and second order resetting can contribute to changes in firing order. One reason that the firing order is not necessarily preserved in the networks in this study is that the new phase versus old phase function for the Wang and Buzsáki model neurons has an initial dip [see Fig. 11(c)] and is therefore not monotonically increasing. A negative phase seems contradictory since the phase is only defined from 0 to 1. We interpret a negative phase as simply indicating that the next spike is not expected for longer than one intrinsic period, since a spike is not generated at a phase of zero but at a phase of 1. The emulator routine accommodates "negative" phases, as can the graphical prediction method, as long as the associated time intervals are nonnegative. The assumption that the resetting is instantaneous causes the apparent negative phase, but in reality, the slowing of the trajectory is distributed over an interval and the phase never actually goes negative. Since we show here that it cannot generally be assumed that firing order will be preserved, more general proofs of synchronization in pulse coupled networks are required.

4.4 Generalize to *N* neuron networks

In networks of real neurons, there will always be heterogeneity and usually near synchrony rather than exact synchrony. There are multiple variations on near synchrony, as shown in this study, and as the network size increases the number of possible variants in terms of phasic relationships and firing order increases. A previous study (Skinner et al. 2005a) found some similarities between two neuron networks and larger networks, and we also identified some similarities. For example, the periodic, near synchronous solutions in which firing order is not preserved are more prevalent at low values of heterogeneity between neurons than at high ones and the 2:2 pattern shifts to 1:1 pattern as the heterogeneity is increased. Although 2:2 patterns exist in networks of more than two neurons, we do not suggest that 2P modes have a distinct, intrinsic functionality, but merely that they can expand the parameter range that supports near synchrony.

4.5 Conclusion

The main result is that PRC methods based on strong coupling give excellent predictions for two neuron heterogenous networks, both in the form of *a priori* theoretical predictions of existence and stability and the phenomenological predictions of the emulator. This extends the applicability of PRC methods beyond those based on the assumptions of weak coupling and mild heterogeneity, which are not invoked here. Another result is that proofs of the stability of synchrony based on the assumption of an invariant firing order also do not apply to pulse coupled neural oscillators because of the readily observed transients and even stable modes in which the firing order is not preserved.

Acknowledgments This work was supported by the NIH grant NS54281 to CCC. We thank Will Curry for assistance with the simulations, and Robert Butera for comments on an earlier draft of the manuscript. We also thank Bard Ermentrout for helpful discussions and the name for the leapfrog mode.

Appendix I: Error minimization approach to finding modes

The minimization approach for the 2:2 lockings in which the firing order does not change was as follows. The values of ϕ_{12} and ϕ_{21} were determined at each point on a grid in the (ϕ_{11}, ϕ_{22}) space as follows by first setting ϕ_{21} equal to $P_1\{1-\phi_{11}+f_{11}(\phi_{11})\}/P_2-f_{22}(\phi_{22})$ per the steady state version of Eq. (3) then setting ϕ_{12} equal to $P_2\{1-\phi_{21}+f_{12}(\phi_{21})\}/P_1-f_{21}(\phi_{11})$ per the steady state version of Eq. (2). In an exact solution, the steady state versions of Eqs. (1) and (4) would be satisfied, thus we utilized the quantities $P_2\{1-\phi_{22}+f_{12}(\phi_{22})\}/P_1-f_{21}(\phi_{12})-\phi_{11}$ and $P_1\{1-\phi_{12}+f_{11}(\phi_{12})\}/P_2-f_{22}(\phi_{21})-\phi_{22}$ as two components of error that must be minimized simultaneously. In a true solution, the value of both errors would fall to zero. All points in the (ϕ_{11}, ϕ_{12}, ϕ_{21}, ϕ_{22}) space generated using Eqs. (2) and (3) were selected if both components of the error from Eqs. (1) and (4) were below a threshold, then all adjacent points on the (ϕ_{11}, ϕ_{22}) grid were considered to form a cluster. The local minimum of the cluster was used as the initial condition for a gradient descent method to find the global minimum on the (ϕ_{11}, ϕ_{22}) grid. If the error threshold was too high, a single cluster might contain two zeroes, but the algorithm would find only one. If the error threshold is set too low, a zero might be missed entirely because none of the grid points are close enough. It is also possible for the algorithm to find a local minimum that is not zero, thus the algorithm must be applied very carefully. This algorithm also finds all 1P modes, since they also satisfy the 2P criteria in which the firing order does not change.

The minimization approach for the 2:2 lockings in which the firing order changes on every cycle was as follows. The values of ϕ_{11} and ϕ_{21} were determined at each point on a grid in the (ϕ_{12}, ϕ_{22}) space as follows by first setting ϕ_{11} equal to $P_2\{1-\phi_{22}+f_{12}(\phi_{22})\}/P_1$ per the steady state version of Eq. (5) then setting ϕ_{21} equal to $P_1\{1-\phi_{12}+$

$f_{11}(\phi_{12})\}/P_2$ per the steady state version of Eq. (7). In an exact solution, Eqs. (6) and (8) would be satisfied, thus we utilized the quantities $\phi_{12}+f_{11}(\phi_{11})-P_2\{1+f_{22}(\phi_{21})+f_{12}(\phi_{22})\}/P_1-\phi_{11}$ and $\phi_{22}+f_{12}(\phi_{21})-P_1\{1+f_{21}(\phi_{11})+f_{21}(\phi_{12})\}/P_2-\phi_{21}$ as two components of error that must be minimized simultaneously, and proceeded as described above.

Appendix II: Details of graphical method

Firing order is preserved

In order to obtain the blue curve in Fig. 4, a loop is performed over all values of φ_{22}. At each value of φ_{22} chosen, the value of φ_{21} that satisfied $ts_{11}=tr_{22}$, $ts_{12}=tr_{21}$, and $ts_{21}=tr_{11}$ was determined. The values of φ_{11} and φ_{12} were also required to determine all of the appropriate intervals. An initial estimate of φ_{11} was obtained by ignoring $f_{21}(\phi_{12}^*)$ in the steady state version of Eq. (1), then an initial estimate of φ_{21} is made using the steady state version of Eq. (3). Then φ_{12} is estimated from the steady state version of Eq. (2). The estimate is refined by repeating the process, now considering rather than ignoring $f_{21}(\phi_{12}^*)$ iteratively until it converges. If there was a solution, the algorithm converged in all cases tested. One problem is that it is possible that there are multiple values of φ_{21} at a given value of φ_{22}, whereas this algorithm would only find one. This rarely caused a problem, however. The choice to plot tr_{22} and ts_{12} as shown in Fig. 4(a) is arbitrary. It is only necessary to pick two intervals for this curve that are equal to two intervals that can be calculated for the other curve as described below.

In order to obtain the red curve in Fig. 4, a loop is performed over all values of φ_{21}. At each value of φ_{21} chosen, the value of φ_{22} that satisfied $ts_{11}=tr_{22}$, $ts_{12}=tr_{21}$, and $ts_{22}=tr_{12}$ was determined. The values of φ_{11} and φ_{12} were also required to determine all of the appropriate intervals. An initial estimate of φ_{12} was obtained by ignoring $f_{21}(\phi_{11}^*)$ in the steady state version of Eq. (2), then an initial estimate of φ_{22} is made using the steady state version of Eq. (4). Then φ_{11} is estimated from the steady state version of Eq. (1). The estimate is refined by repeating the process, now considering rather than ignoring $f_{21}(\phi_{11}^*)$ iteratively until it converges. It should be noted that in order to interpolate properly, the intersections were actually calculated in the (φ_{21}, φ_{22}) plane, then the values of φ_{11} and φ_{12} were calculated at the intersection, and these values were used to predict the intervals observed in each mode. It was necessary to check that all calculated phases were in the range 0 to 1 and that the calculated intervals were nonnegative.

Firing order is not preserved

In order to obtain the red curve in Fig. 5, a loop was performed over all values of φ_{12}, and the values of ϕ_{22} that satisfied $ts_{11}=tr_{21}$, $ts_{21}=tr_{11}$, and $ts_{22}=tr_{12}$ was determined. First the value of φ_{21} was determined from the steady state version of Eq. (7). Then a loop was performed through the values of φ_{22} with φ_{11} set to the value determined by the steady state version of Eq. (5) in order to find all the values of φ_{22} that satisfied the steady state version of Eq. (8). The values of the phases so determined were used to compute tr_{12} and ts_{12} as shown. Multiple values of φ_{22} were sometimes found, and due to the way in which the loop is structured, points on the same branch may not be found in sequential order, but rather intermixed with points on other branches. Since the plot is a planar section of a four dimensional space, there is no guarantee that all branches are actually coplanar, thus care must be exercised in using these plots. Again, it was necessary to check that all calculated phases in the range of 0 to 1 and that the intervals are nonnegative only in a limited range of values.

In order to obtain the blue curve in Fig. 5, a loop was performed over all values of φ_{22}, and the values of φ_{12} that satisfied $ts_{11}=tr_{21}$ $ts_{12}=tr_{22}$, and $ts_{21}=tr_{11}$ was determined. First the value of φ_{11} was determined from the steady state version of Eq. (5). Then a loop was performed through the values of φ_{12} with φ_{21} set to the value determined by the steady state version of Eq. (7) in order to find all the values of φ_{22} that satisfied the steady state version of Eq. (6). The values of the phases so determined were used to compute ts_{22} and tr_{22} as shown. Again, the actual intersections were calculated in the (φ_{12}, φ_{22}) plane to facilitate interpolation.

References

Bartos, M., Vida, I., Frotscher, M., Geiger, J. R. P., & Jonas, P. (2001). Rapid signaling at inhibitory synapses in a dentate gyrus interneuron network. *Journal of Neuroscience*, *21*, 2687–2698.

Bartos, M., Vida, I., Frotscher, M., Meyer, M., Monyer, H., Geiger, J. R. P., et al. (2002). Fast synaptic inhibition promotes synchronized gamma oscillations in hippocampal interneuron networks. *Proceedings of the National Academy of Sciences of the United States of America*, *99*, 13222–13227.

Canavier, C. C., Baxter, D. A., Clark, J. W., & Byrne, J. H. (1999). Control of multistability in ring circuits of oscillators. *Biological Cybernetics*, *80*, 87–102.

Canavier, C. C., Butera, R. J., Dror, R. O., Baxter, D. A., Clark, J. W., & Byrne, J. H. (1997). Phase response characteristics of model neurons determine which patterns are expressed in a ring circuit model of gait generation. *Biological Cybernetics*, *77*, 367–380.

Dror, R. O., Canavier, C. C., Butera, R. J., Clark, J. W., & Byrne, J. H. (1999). A mathematical criterion based on phase response curves for stability in a ring of coupled oscillators. *Biological Cybernetics*, *80*, 11–23.

Ermentrout, B. (1996). Type I membranes, phase resetting curves, and synchrony. *Neural Computation*, *8*, 979–1002.

Ermentrout, B. (2002). *Simulating, analyzing, and animating dynamical systems: A guide to XPPAUT for researchers and students*. Philadelphia, PA: SIAM.

Goel, P., & Ermentrout, B. (2002). Synchrony, stability, and firing patterns in pulse-coupled oscillators. *Physica D*, *163*, 191–216.

Guevara, M. R., Shrier, A., & Glass, L. (1986). Phase resetting of spontaneously beating embrionic ventricular heart cell aggregates. A. *Journal of Physiology*, *251*(Heart Circ. Physiol. 20), H1298–H1305.

Hairer, E., & Wanner, G. (1991). *Solving Ordinary Differential Equations II. Stiff and Differential-algebraic Problems. Springer Series in Comput. Mathematics* (Vol 14). Berlin: Springer.

Kopell, N. (1987). Toward a theory of modelling central pattern generators. In A. H. Cohen, S. Grillner, & S. Rossignol (Eds.), *Neural control of rhythmic movements in vertebrates*. (pp. 369–413). New York: Wiley.

Luo, C., Canavier, C. C., Baxter, D. A., Byrne, J. H., & Clark, J. W. (2004). Multimodal Behavior in a four neuron ring circuit: Mode switching. *IEEE Transactions on Biomedical Engineering*, *51*, 205–218.

Marder, E. E., & Calabrese, R. L. (1996). Principles of rhythmic motor pattern generation. *Physiological Reviews*, *76*, 687–717.

Mirollo, R. E., & Strogatz, S. H. (1990). Synchronization of pulse coupled biological oscillators. *SIAM Journal on Applied Mathematics*, *50*, 1645–1662.

Netoff, T. I., Acker, C. D., Bettencourt, J. C., & White, J. A. (2005a). Beyond two-cell networks: Experimental measurement of neuronal responses to multiple synaptic inputs. *Journal of Computational Neuroscience*, *18*, 287–295.

Netoff, T. I., Banks, M. I., Dorval, A. D., Acker, C. D., Haas, J. S., Kopell, N., et al. (2005b). Synchronization in hybrid neuronal networks of the hippocampal formation. *Journal of Neurophysiology*, *93*, 1197–1208.

Oprisan, S. A., & Canavier, C. C. (2001). Stability analysis of rings of pulse-coupled oscillators: The effect of phase-resetting in the second cycle after the pulse is important at synchrony and for long pulses. *Differential Equations and Dynamical Systems*, *9*, 243–258.

Oprisan, S. A., & Canavier, C. C. (2002). The influence of limit cycle topology on the phase resetting curve. *Neural Computation*, *14*, 1027–1057.

Oprisan, S. A., Prinz, A. A., & Canavier, C. C. (2004). Phase resetting and phase locking in hybrid circuits of one model and one biological neuron. *Biophysical Journal*, *87*, 2283–2298.

Pervouchine, D. D., Netoff, T. I., Rotstein, H. G., White, J. A., Cunningham, M. O., Whittington, M. A., et al. (2006). Low-dimensional maps encoding dynamics in entorhinal cortex and hippocampus. *Neural Computation*, *18*, 1–34.

Preyer, A., & Butera, R. J. (2005). Neural oscillators in *Aplysia californica* that demonstrate weak coupling *in vitro*. *Physical Review Letters*, *95*(13), 138103.

Reyes, A. D., & Fetz, E. E. (1993). Two modes of interspike interval shortening by brief transient depolarizations in cat neocortical neurons. *Journal of Neurophysiology*, *69*, 1661–1672.

Rinzel, J., & Ermentrout, B. (1998). Analysis of neural excitability and oscillations. In C. Koch & I. Segev (Eds.), *Methods in neuronal modeling from ions to networks*. Cambridge, MA: MIT Press.

Skinner, F. K., Bazzazi, H., & Campbell, S. A. (2005a). Two-cell to N-cell heterogenous, inhibitory networks, precise linking of multistable and coherent properties. *Journal of Computational Neuroscience*, *18*, 343–352.

Skinner, F. K., Chung, J. Y., Ncube, I., Murray, P. A., & Campbell, S. A. (2005b). Using heterogeneity to predict inhibitory network model characteristics. *Journal of Neurophysiology*, *93*, 1898–1907.

Strogatz, S. H. (2000). From Kuramoto to Crawford: Exploring the onset of synchronization in populations of coupled oscillators. *Physica D*, *143*, 1–2.

Wang, X. J., & Buzsáki, G. (1996). Gamma oscillation by synaptic inhibition in a hippocampal interneuronal network model. *Journal of Neuroscience*, *16*, 6402–6413.

White, J. A., Chow, C. C., Ritt, J., Soto-Trevino, C., & Kopell, N. (1998). Synchronization and oscillatory dynamics in heterogeneous, mutuallly inhibited neurons. *Journal of Computational Neuroscience*, *5*, 5–16.

Whittington, M. A., Traub, R. D., & Jefferys, J. G. (1995). Synchronized oscillations in interneuron networks driven by metabotropic glutamate receptor activation. *Nature*, *373*, 612–615.